

1 **Spatio-temporal coherence of circadian clocks and gating of**
2 **differentiation in *Anabaena* filaments**

3
4 Rinat Arbel-Goren^{1*}, Bareket Dassa², Anna Zhitnitsky¹, Ana Valladares³, Antonia Herrero³,
5 Enrique Flores^{3*} and Joel Stavans^{1*}

6
7
8 ¹Department of Physics of Complex Systems
9 ²Department of Life Sciences Core Facilities
10 Weizmann Institute of Science
11 Rehovot 76100, Israel

12
13 ³Instituto de Bioquímica Vegetal y Fotosíntesis,
14 CSIC and Universidad de Sevilla,
15 Américo Vespucio 49, E-41092 Seville, Spain

16
17
18
19
20
21
22 * Corresponding authors

Abstract

23

24

25 Circadian clock arrays in multicellular filaments of the heterocyst-forming cyanobacterium
26 *Anabaena* sp. strain PCC 7120 display remarkable spatio-temporal coherence under nitrogen-
27 replete conditions. To shed light on the interplay between circadian clocks and the formation of
28 developmental patterns, we followed the expression of a clock-controlled gene under nitrogen
29 deprivation, at the level of individual cells. Our experiments showed that differentiation into
30 heterocysts took place preferentially within a limited interval of the circadian clock cycle; that
31 gene expression in different vegetative intervals along a developed filament was discoordinated;
32 and that the circadian clock was active in individual heterocysts. Furthermore, *Anabaena*
33 mutants lacking the *kaiABC* genes encoding the circadian clock core components produced
34 heterocysts but failed in diazotrophy. Therefore, genes related to some aspect of nitrogen
35 fixation, rather than early or mid-heterocyst differentiation genes, are likely affected by the
36 absence of the clock. A bioinformatics analysis supports the notion that RpaA may play a role as
37 master regulator of clock outputs in *Anabaena*, the gating of differentiation by the circadian
38 clock and the involvement of the clock in proper diazotrophic growth. Together, these results
39 suggest that under nitrogen deficient conditions, the functional unit in *Anabaena* is reduced
40 from a full filament under nitrogen-rich conditions, to the vegetative cell interval between
41 heterocysts.

42

43 Introduction

44 Circadian clocks arose during evolution to enable organisms, from cyanobacteria to plants and
45 mammals, to tune their metabolism and bioprocesses to daily light/darkness cycles on Earth,
46 and thereby optimize their fitness (Johnson and Rust, 2021; Shultzaberger et al., 2015). Much of
47 what is known about the mechanisms behind circadian clocks in the case of cyanobacteria has
48 been learned from investigations of unicellular organisms, primarily *Synechococcus elongatus*
49 strain PCC 7942 (henceforth *S. elongatus*). These investigations have firmly established that the
50 core clock is comprised of three proteins, KaiA, KaiB and KaiC, the first two of which modulate
51 the four phosphorylation states of KaiC, which cycle with time. The information encoded in the
52 phosphorylation state of KaiC is then relayed to clock-controlled genes by the master
53 transcription factor RpaA (Markson et al., 2013; Taniguchi et al., 2010) via the input/output
54 sensor histidine kinases CikA and SasA, the phosphatase and kinase that modulate RpaA activity
55 (Cohen, 2020). KaiA and KaiB regulate the phosphorylation state of KaiC in a negative feedback
56 loop configuration that drives the oscillatory gene expression. In addition to the elucidation of
57 many mechanistic details (Cohen, 2020), other investigations have provided evidence indicating
58 that that the circadian clock in *S. elongatus* gates the cell cycle (Dong et al., 2010; Yang et al.,
59 2010) and regulates the competence state, natural transformation being maximal when the
60 onset of darkness coincides with the dusk circadian peak (Taton et al., 2020).

61 An important cyanobacterial order, *Nostocales*, consists of multicellular organisms such
62 as *Anabaena* sp. strain PCC 7120 (henceforth *Anabaena*), in which cells are organized in a
63 filamentary structure, with local, nearest-neighbor cell-cell coupling via septal junctions (Herrero
64 et al., 2016). *Anabaena* bears homologs not only of the core *kai* genes of *S. elongatus*
65 (Schmelling et al., 2017), but also of the network of genes in which they are embedded, and
66 those coding for RpaA, as well as CikA and SasA. Whereas not much is known about the detailed
67 molecular mechanisms behind the circadian clock in *Anabaena*, structural studies suggest that
68 the interactions between the respective proteins are similar (Garces et al., 2004).

69 First insights into the dynamical behavior of clocks in *Anabaena* were obtained from
70 bulk and DNA microarray studies that established that its circadian clock is autonomous, and
71 that it can run freely under constant light conditions (Kushige et al., 2013). Following
72 entrainment by two 12-h light-dark cycles, a group of genes exhibiting oscillatory behavior were
73 identified, and the homologs of *kaiA*, *kaiB*, and *kaiC* genes showed low-amplitude or arrhythmic
74 expression, in contrast to those of *S. elongatus* (Kushige et al., 2013). More recently, the

75 collective behavior of circadian clocks in *Anabaena* filaments has been studied at the individual
76 cell level (Arbel-Goren et al., 2021). Circadian clocks along filaments were interrogated under
77 nitrogen-replete conditions in which all cells in the filaments were vegetative, carrying out both
78 oxygenic photosynthesis and assimilation of a source of combined nitrogen. Under these
79 conditions, filaments grow by binary fission of each and every cell along their length. This study
80 found significant synchronization and spatial coherence of clock phases on the scale of
81 filaments, evidence supporting the notion of clock coupling via cell-cell communication, and
82 gating of the cell division by the circadian clock. Furthermore, the study confirmed the low-
83 amplitude circadian oscillatory transcription of *kai* genes comprising the post-transcriptional
84 core oscillatory circuit suggested by results of a bulk study (Kushige et al., 2013), and found
85 evidence of large-amplitude oscillations of *rpaA* transcription (Arbel-Goren et al., 2021).

86 Under nitrogen deficient conditions, *Anabaena* fixes atmospheric nitrogen, an activity that
87 is incompatible with the oxygen produced by photosynthesis (Flores and Herrero, 2010). The
88 incompatibility of photosynthesis and nitrogen fixation is solved by division of labor: filaments
89 undergo a process of development into a one-dimensional pattern consisting of single,
90 specialized micro-oxic cells, the heterocysts, in which atmospheric nitrogen fixation takes place,
91 separated by about 10-15 vegetative cells that fix CO₂ photosynthetically (Corrales-Guerrero et
92 al., 2015; Di Patti et al., 2018; Herrero et al., 2016). The genetic cascade leading to heterocyst
93 formation is controlled by the master regulator of differentiation HetR, and involves at least two
94 inhibitory signals related to the PatS polypeptide and the HetN protein that can be transferred
95 from cell to cell through septal junctions. Heterocyst differentiation and the ensuing emergence
96 of developmental patterns in *Anabaena* entail profound metabolic and morphological changes
97 (Flores et al., 2019; Herrero et al., 2016), including some that affect cell-cell communication
98 (Camargo et al., 2021). Results from a DNA microarray analysis of heterocyst-enriched samples
99 have provided evidence of circadian clock activity of *kai* genes in heterocysts (Kushige et al.,
100 2013). However, the possibility that the rhythmic transcription was indirectly induced in
101 heterocysts by time-dependent intercellular signals from oscillators in neighboring vegetative
102 cells could not be excluded. Moreover, the results revealed that under nitrogen deficient
103 conditions, 39 of the 78 previously identified clock-controlled genes preserved rhythmic
104 expression, a subset being heterocyst-specific (Kushige et al., 2013). Of note, the number of
105 genes reported to oscillate with a circadian period in *S. elongatus* is 856, significantly larger than
106 78 (Markson et al., 2013).

107 Here we set out to study the interplay between the circadian clock and the genetic
108 network controlling heterocyst differentiation under nitrogen deficient conditions in *Anabaena*.
109 We tracked circadian rhythms in individual vegetative cells and heterocysts in combined
110 nitrogen-deprived *Anabaena* filaments in real time, by following the expression from the
111 promoter of *pecB*, a clock-controlled gene that exhibits high-amplitude oscillations (Kushige et
112 al., 2013). This gene is part of the *pecBACEF* operon coding for the beta subunits of
113 phycoerythrocyanin, a structural component of the phycobilisome rod that plays a major role in
114 light harvesting for photosynthesis (Swanson et al., 1992). Our study provides evidence that
115 nitrogen deprivation has a profound influence on the synchronization and spatial coherence of
116 clocks along a filament, and that in addition to gating the cell cycle, the circadian clock also gates
117 cellular differentiation.

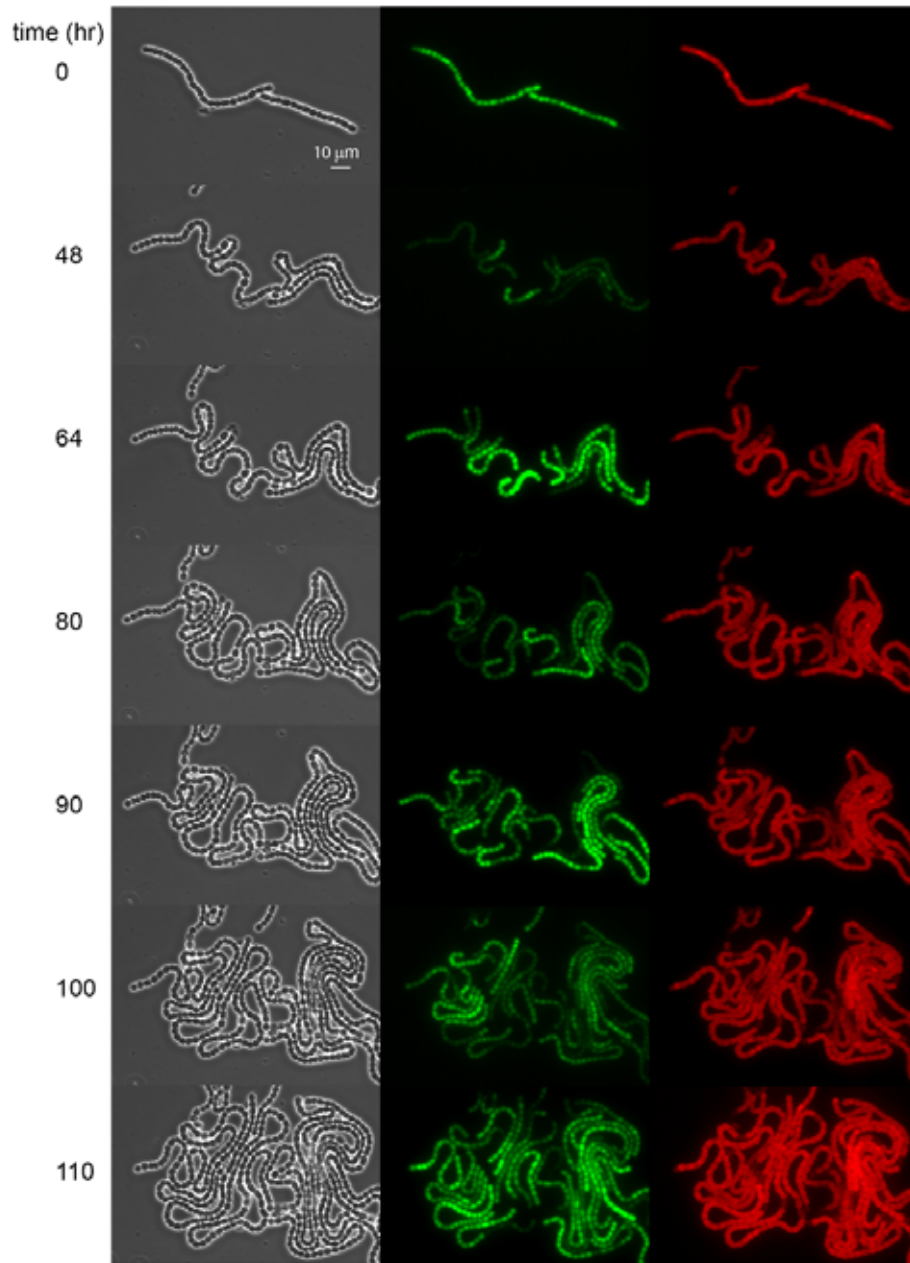
118

119 **Results**

120 **Discoordinated expression of a clock-controlled gene along filaments under constant light**
121 **conditions.** The *pecB* gene, encoding the beta subunit of phycoerythrocyanin (Swanson et al.,
122 1992), is known to display circadian oscillations both under nitrogen-replete and nitrogen
123 deficient conditions (Kushige et al., 2013). Expression from a chromosomal fusion of *gfp* to the
124 5' region of *pecB*, denoted as $P_{pecB-gfp}$ (13), was followed along wild-type *Anabaena* filaments
125 under constant light, after submitting filaments to nitrogen deprivation in BG11₀ medium. A
126 series of phase contrast, fluorescence and autofluorescence of photosynthetic pigments (AF)
127 snapshots taken at maxima and minima of a number of circadian cycles is shown in Fig. 1. In
128 contrast to the images taken right after nitrogen deprivation (t=0), in which expression along a
129 filament was largely uniform except for small amplitude variations, at later times filaments
130 displayed considerable heterogeneity. This heterogeneity may be due to demographic noise, or
131 alternatively, may reflect different metabolic states in different cell stretches of the filament
132 (Nieves-Mori3n et al., 2021). Expression from $P_{pecB-gfp}$ was visibly higher in some vegetative
133 intervals than in others, alternating in time, and the heterogeneity in expression was spatially
134 locked with the instantaneous pattern of heterocysts to a large extent (Fig. 1, Movie 1).

135 The physiological changes involved in the differentiation of a vegetative cell into a
136 heterocyst entail alteration of cell-cell communication (Herrero et al., 2016), and altered cell-cell
137 communication (Ar3valo et al., 2021) may lead to the presence of filament cell stretches
138 showing different metabolic states (Nieves-Mori3n et al., 2021). To test the notion that altered

139 communication may affect the synchrony along a filament, we evaluated the extent of
140 synchronization between vegetative cells belonging to different vegetative intervals, and
141 compared it to the synchronization of vegetative cells within the same interval. To this end, we
142 calculated the synchronization index R (Materials and Methods and (Garcia-Ojalvo et al., 2004))
143



144





145

146

147 **Figure 1. Circadian oscillations in *Anabaena* filaments under nitrogen-poor conditions.** (Left)
 148 Phase contrast images of a filament of an *Anabaena* strain, growing under nitrogen-poor
 149 conditions. (Middle) GFP fluorescence in a filament of an *Anabaena* strain bearing a P_{pecB} -*gfp*
 150 promoter fusion, growing under nitrogen-poor conditions. (Right) Autofluorescence as a
 151 function of time in *Anabaena*. Snapshots correspond to those in the left-hand micrographs and
 152 time 0 corresponds to the time at which filaments were placed under the microscope. The times
 153 at which snapshots were taken were chosen near maxima and minima of the circadian
 154 oscillations observed in GFP fluorescence intensity. For a time-lapse movie see Movie 1.
 155

156 between the two vegetative cells on either side of a given heterocyst, and compared its value to
 157 R calculated for two vegetative cells separated by an intervening vegetative cell (Table 1, second
 158 and third rows).

159

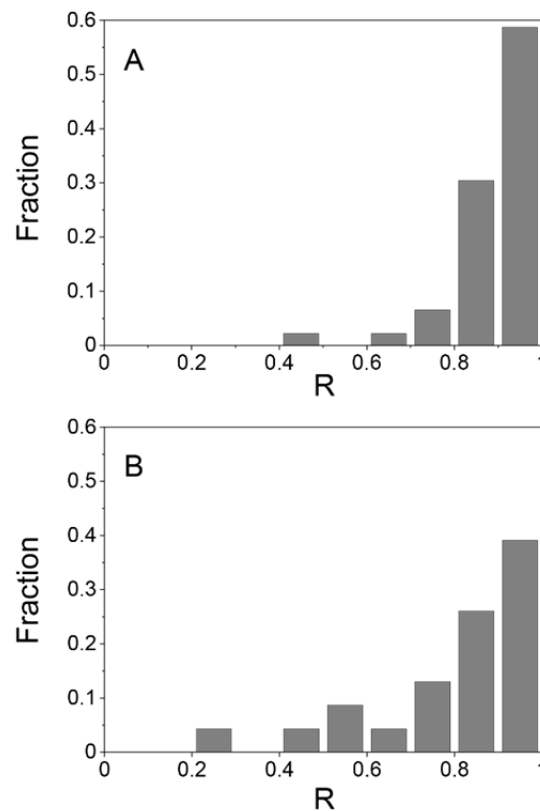
Cell cluster	R (Mean \pm SEM)	Cells over which R was calculated
Contiguous vegetative	0.80 \pm 0.03	
Pair-wise around heterocyst	0.79 \pm 0.19	
Pair-wise around vegetative	0.90 \pm 0.1	
One cell per vegetative interval	0.44 \pm 0.15	

160

161 **Table 1. Synchronization index R of vegetative cells under nitrogen-poor conditions.** The
 162 synchronization index R (Materials and methods) of vegetative cells within filaments under
 163 nitrogen-poor conditions is shown. First row: all contiguous vegetative cells within heterocyst-
 164 bounded intervals (10 cells per interval and three independent intervals). Second row: pairs of
 165 vegetative cells separated by a heterocyst (4 pairs, three independent experiments). Third row:
 166 pairs of vegetative cells separated by a single vegetative cell (4 pairs, three independent
 167 experiments). Fourth row: two vegetative cells adjacent to two heterocysts in different intervals
 168 (10 cells per filament, three independent experiments). Values of R represent means over the
 169 indicated number of independent experiments, and errors represent the standard errors.
 170 Yellow cells in the respective cartoons represent the vegetative cells in filaments over which R
 171 was calculated in each case. Dark green cells represent heterocysts and light green represent
 172 vegetative cells.

173

174 While the mean values of R in both cases were comparable, the distributions of R values were
175 highly skewed (Fig. 2). A comparison using a Wilcoxon-Mann-Whitney test indicates that these
176 distributions differ significantly at the $p < 0.009$ level. In addition, we compared the relative
177 synchronization of vegetative intervals at the level of the whole filament. We obtained R
178 $= 0.44 \pm 0.15$ for cells from different vegetative intervals and $R = 0.80 \pm 0.03$ from those within the
179 same interval, under nitrogen-deprived conditions (Table 1). This is compared to $R = 0.59 \pm 0.06$



180 and $R = 0.85 \pm 0.01$ under nitrogen-rich conditions for separated cells in different filaments and
181 the

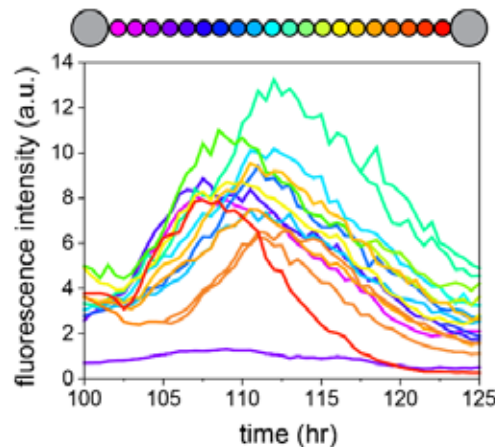
182

183 **Figure 2. Distribution of R values between separated cells.** Pair-wise values of R between
184 vegetative cells separated by a single vegetative cell (A) or heterocyst (B). The mean and SD of
185 the distributions from at least two independent experiments are: $R = 0.90 \pm 0.1$ and $R = 0.79 \pm$
186 0.19 respectively. A Wilcoxon-Mann-Whitney U-test indicates that these data come from
187 continuous distributions with different medians with $p = 0.0086$ at the 5% significance level.
188

189 same filament respectively (Arbel-Goren et al., 2021). These findings indicate that, in
190 diazotrophic filaments, oscillations in vegetative intervals are desynchronized from one another,
191 much like cells from entirely separate filaments, but maintain a normal degree of synchrony
192 within intervals.

193 **Sequential turnoff of expression in vegetative cells between consecutive heterocysts.** A salient
194 feature of oscillations in the fluorescence intensity from P_{pecB} -*gfp* was the cell-cell variation in
195 the times at which expression was turned off in vegetative cell intervals, preempting the
196 decrease of the fluorescence intensity and the completion of a cycle. This decrease, mediated
197 presumably both by dilution by cell growth and degradation of the GFP, resulted in a particularly
198 wide spread of fluorescence intensity values between cells. To check whether there is
199 coordination in expression turnoff times along a filament, we represented the fluorescence
200 intensity in individual contiguous cells in a heterocyst-bound interval during one oscillation,
201 color-coded according to

202 their spatial position along the vegetative interval (Fig. 3). Notably, the fluorescence intensity

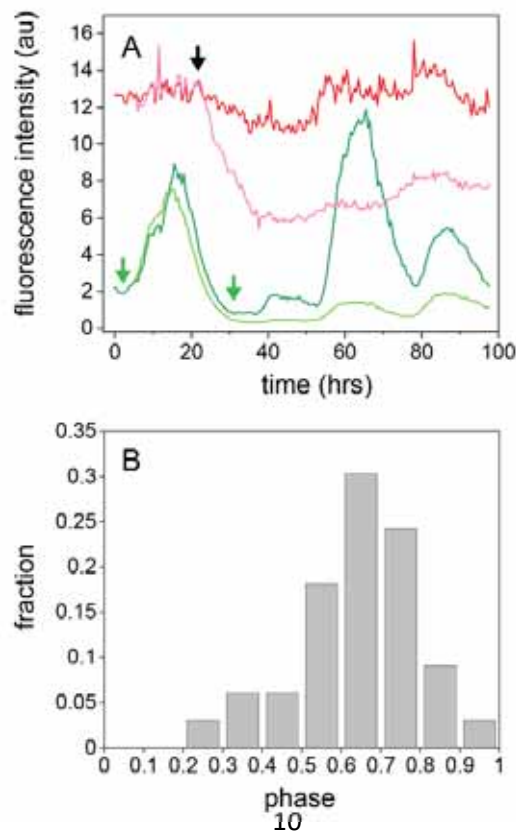


203 **Figure 3. Gradient and sequential activation of fluorescence intensity from P_{pecB} -*gfp* of**
204 **vegetative cells within a heterocyst-bound interval.** Fluorescence intensity of individual cells as
205 a function of time over one circadian cycle. Traces are color-coded according to their position
206 along a heterocyst-bound vegetative interval. The violet line at the bottom of the plot
207 corresponds to the trace of one of the bounding heterocysts.

208 during upregulation was synchronized among cells, but the decay was delayed as a function of
209 the cell's proximity to a heterocyst. Thus the decay in cells near the middle of a vegetative
210 interval was most delayed. We did not detect sequential turnoff under nitrogen-replete
211 conditions. Note also that cells near the middle of the vegetative interval appear to display
212 higher expression.

213 **The circadian clock gates heterocyst differentiation.** To test whether the heterocyst
214 differentiation process and circadian clocks are temporally coordinated in *Anabaena* cells, we
215 determined the onset of the reduction of the autofluorescence of photosynthetic pigments (AF)
216 in a cell that eventually will become a heterocyst as a temporal reference point (Foulds and
217 Carr, 1977; Maldener et al., 1991; Wood and Haselkorn, 1980), and its phase along the cell's
218 circadian cycle, taking 0 and 2π to correspond to consecutive minima in the cyclic expression
219 from P_{pecB} -*gfp* (Fig. 4A). A histogram of the phases of AF intensity reduction events obtained
220 from traces similar to those in Fig. 4A is shown in Fig. 4B. Clearly, differentiation takes place
221 within a narrow temporal window of the circadian cycle. We conclude that the circadian clock
222 gates heterocyst differentiation. Lastly, we note that the phase of oscillation in the heterocyst
223 was inherited from that of the original vegetative cell.

224 **Low amplitude circadian oscillations in heterocysts.** Evidence for circadian clock activity in
225 heterocysts was obtained previously by interrogating heterocyst-enriched bulk samples (Kushige
226 et al., 2013). However, these experiments could not exclude the possibility that oscillations were
227 induced in heterocysts from the transfer of time-dependent signals from neighboring vegetative
228 cells. To test whether oscillating transcription indeed takes place in heterocysts, we followed

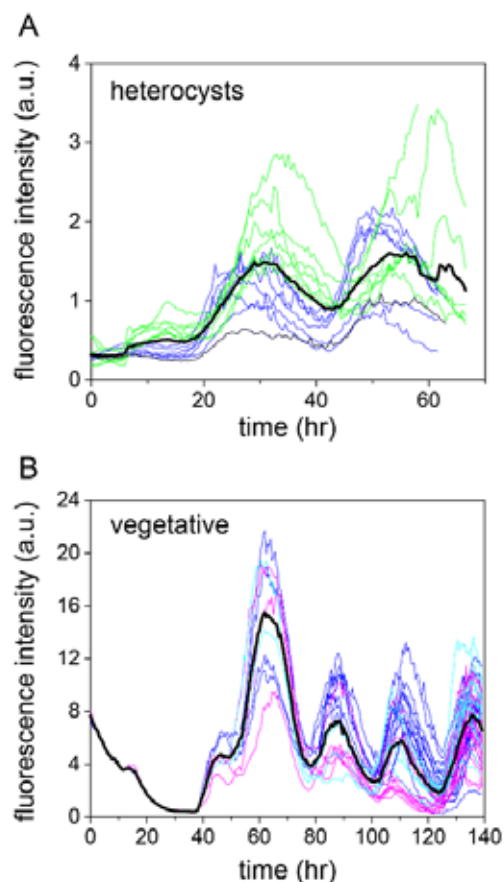


229 expression from

230

231 **Figure 4. Gating of heterocyst differentiation by the circadian clock.** (A) Fluorescence
232 intensities of two sister cells bearing a P_{pecB} -*gfp* fusion (green) one of which eventually becomes
233 a heterocyst, and their respective autofluorescence intensity traces (red) as a function of time,
234 under conditions of constant illumination. The onset in the decay of autofluorescence (AF) in the
235 cell that becomes a heterocyst is indicated with a black arrow, whereas the positions of the
236 circadian cycle minima on either side are indicated with green arrows. (B) Normalized histogram
237 of the phase of onset times of autofluorescence reduction in cells that become heterocysts, with
238 0 and 1 denoting two consecutive minima in circadian cycles in units of 2π . Data from at least
239 three independent experiments.

240 P_{pecB} -*gfp* in individual heterocysts that formed after filaments were subjected to nitrogen
241 deprivation (BG11₀ medium). The fluorescence intensity of individual heterocysts in a typical
242 experiment is shown in Fig. 5A. Since heterocysts formed at different times during the
243 experiment, traces have been temporally aligned by using the onset of the decay in the



244 autofluorescence as a temporal reference point (Foulds and Carr, 1977; Maldener et al., 1991;
245 Wood and Haselkorn, 1980) (e.g., Fig. 5A). A comparison of these traces with those of three
246 vegetative cells and their respective lineages (Fig. 5B) shows that the period of the oscillations in

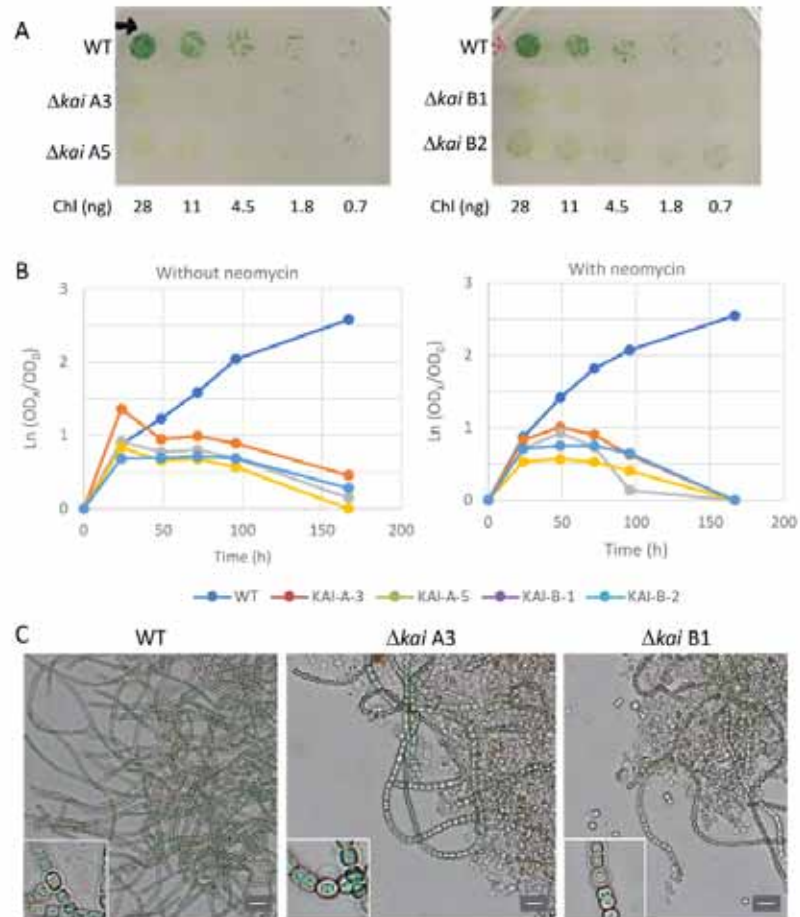
247 heterocysts (21.3 ± 0.6 mean \pm SE $n=30$) is undistinguishable from that observed in vegetative
248 cells (20.8 ± 0.4 , mean \pm SE $n=35$), and that their amplitude is about a factor of five smaller.

249

250 **Figure 5. Fluorescence intensity from P_{pecB} -*gfp* as a function of time in heterocysts and**
251 **vegetative cell lineages.** (A) Fluorescence intensity in heterocysts. Different colors correspond
252 to data from different filaments. Traces were displaced so that the onsets of decay of
253 autofluorescence in the vegetative cells that differentiate into heterocysts coincide. (B) Lineages
254 of three cells each in one of three contiguous vegetative cell intervals (color-coded according to
255 their respective interval). Thick black lines in both panels correspond to the average of all
256 traces.

257

258 **Δkai mutant filaments fail to grow fixing N_2 .** To understand further the role played by the
259 circadian clock in filament behavior under nitrogen deprivation, we studied the phenotype of
260 filaments in which *kaiABC* genes were deleted (henceforth $\Delta kaiABC$ strains, Fig. S1). The growth
261 of a $\Delta kaiABC$ strain was studied using four independent clones: two in which the C.K1 gene
262 cassette was inserted in direct orientation (clones A) and two in which it was inserted in reverse
263 orientation (clones B) with regard to the orientation of the operon. None of the clones could
264 grow under photoautotrophic conditions in solid BG11₀ medium, which lacks combined nitrogen
265 (Fig. 6A). In liquid BG11₀ medium, after an initial increase in cell mass, the four clones also failed
266 to grow (Fig. 6B). Ten days after nitrogen deprivation, cultures from two clones bearing the
267 inserted cassette in each of the two possible orientations were visualized by light microscopy,
268 showing the presence of abundant cell debris and few filaments as compared to the WT (Fig.
269 6C). Nonetheless, heterocysts were observed in the two mutant cultures as in the WT culture,
270 and the frequency of heterocysts was similar in the three cultures, albeit slightly higher in the
271 mutants than in the WT at 24 h and slightly lower at 48 h (Fig. S2). Furthermore, filaments of
272 $\Delta kaiABC$ strains exhibited a significantly lower production of photosynthetic pigments under
273 nitrogen deprivation relative to the wild-type strain (Fig. 6A), precluding the detection of the
274 decay of autofluorescence in incipient heterocysts. These observations collectively show that
275 deletion of the *kai* genes leads to failure in diazotrophic growth while allowing heterocyst
276 differentiation.



277

278 **Figure 6. Phenotype of the Δkai mutants of *Anabaena sp.* strain PCC 7210.** (A) Growth tests on
 279 plates with BG11₀ medium. The filaments were grown in BG11 medium with neomycin at 20 μg
 280 mL^{-1} , washed with BG11₀ medium (without neomycin), and incubated in BG11₀ medium
 281 (without neomycin) for 10 days under photoautotrophic culture conditions. (B) Growth tests in
 282 liquid BG11₀ medium without neomycin or with neomycin at 20 μg mL^{-1} for the mutants, as
 283 indicated. y axis, Ln (OD₇₅₀ nm at time X/OD₇₅₀ nm at time 0); x axis, time of incubation under
 284 photoautotrophic culture conditions. For panels A and B, the wild type (WT) and two mutant
 285 clones from each orientation of the gene cassette were analyzed. (C) Bright field micrographs of
 286 the WT and Δkai mutant (clones A3 and B1) after 10 days of incubation in BG11₀ medium.
 287 Whereas the WT formed long filaments, much cell debris and only a few filaments were
 288 observed for the mutants. Size bar, 10 μm . Insets, further magnification (5x) showing the
 289 presence of heterocysts in the three strains.

290

291 **Candidate genes linking the circadian clock to the behavior of *Anabaena* under nitrogen**
 292 **deprivation.** To shed light on the relationship between gating of differentiation and the failure
 293 in diazotrophy of $\Delta kaiABC$ strains on one hand, and the circadian clock on the other, we
 294 searched bioinformatically the *Anabaena* genome for a conserved signature of the RpaA-binding

295 motif previously reported for 101 sequences in *S. elongatus* (Markson et al., 2013), taking
296 advantage of the 96% similarity between the RpaA amino acid sequence of *S. elongatus* and
297 *Anabaena* RpaA protein (All0129). Our search was restricted to detect the motif only within
298 regions starting upstream to putative transcription start sites (TSSs) of genes, based on reported
299 annotations of TSS (Mitschke et al., 2011) (motifs within a window of -500bp to +50bp relative
300 to the TSS).

301 A number of genes encoding regulatory proteins were detected among 81 genes bearing
302 putative RpaA binding sites with a FIMO q-value < 0.05 (Table S1). These include the ferric
303 uptake regulator-related protein FurC (Alr0957), which is a protein with pleiotropic effects that
304 affects nitrogen fixation in *Anabaena* (Sarasa-Buisan et al., 2022); the cAMP-binding
305 transcriptional regulator Alr2325 (Suzuki et al., 2004); and the RNA polymerase sigma factor
306 SigE, which is involved in expression of late heterocyst-specific genes (Mella-Herrera et al.,
307 2011). Additionally, four other transcriptional regulators including a transcriptional regulator of
308 unknown function (Alr3646) and three two-component regulators (All3822, Alr5272, Alr5069)
309 were detected. It will be of interest to investigate in the future whether these regulators are
310 indeed involved in circadian clock-related activities.

311

312 Discussion

313 Cells in *Anabaena* filaments exhibit robust circadian rhythms under both nitrogen replete and
314 deficient conditions. However, the single-cell observations reported here demonstrate that the
315 behavior under both conditions differs considerably. Rather than displaying the high synchrony
316 and spatial coherence characteristic of filaments under nitrogen-replete conditions (Arbel-Goren
317 et al., 2021), filaments under nitrogen deprivation display noticeable differences in the phase of
318 expression of a clock-controlled gene between different vegetative cell intervals when
319 compared to the phase synchrony within the interval. The physiological changes involved in the
320 differentiation of a cell into a heterocyst entail alteration of cell-cell communication breaking
321 the symmetry of intercellular transfer: heterocysts become a sink of carbohydrates supplied by
322 their vegetative neighbors, whereas heterocysts supply fixed nitrogen products to the
323 neighboring vegetative cells (Herrero et al., 2016). The discoordination between vegetative
324 filaments together with the reduced communication between vegetative cell intervals suggest
325 that a vegetative cell interval and its delimiting heterocysts is the organismic unit in *Anabaena*

326 under nitrogen fixing conditions, instead of the full filament as in nitrogen-replete conditions.
327 This is further supported by the observation that heterocyst differentiation is not synchronized
328 at the level of the whole filament under steady diazotrophic conditions.

329 A number of cellular processes have been reported to be regulated by circadian clocks in
330 cyanobacteria. For example, the cell cycle is gated both in unicellular *S. elongatus* (Dong et al.,
331 2010; Yang et al., 2010) as well as in *Anabaena* (Arbel-Goren et al., 2021). Similarly,
332 experimental evidence supports the notion that the competence state in *S. elongatus* is
333 regulated by the circadian clock (Taton et al., 2020). Here we found that the circadian clock also
334 gates differentiation of vegetative cells into heterocysts, and that $\Delta kaiABC$ background filaments
335 are impaired in diazotrophic growth. The fitness benefit of gating differentiation by the circadian
336 clock is unclear, but we can surmise that the metabolic load on the cell may be minimized by
337 avoiding differentiation during periods in which the cell is engaged in other processes that may
338 compete with it. This notion is consistent with our observation that most differentiation events
339 occur primarily when cell division events are infrequent (Arbel-Goren et al., 2021), and with the
340 possibility that cell division of mother cells is not an essential requirement for heterocyst
341 differentiation after nitrogen step-down (Asai et al., 2009). This possibility is under current
342 discussion. The fact that the phase of the clock in a heterocyst is inherited from the progenitor
343 cell, when compared to the phase of the clock of the progenitor's sister cell, indicates that while
344 the clock gates differentiation, the clock itself is rather insensitive to the differentiation process,
345 despite the attendant metabolic changes involved in the differentiation process.

346 Interestingly, the absence of a clock does not prevent differentiation of (non-functional)
347 heterocysts. A possible clue that may point to a mechanism behind gating of differentiation by
348 the circadian clock is furnished by the 5-10-fold reduction in the levels of *pecB* transcription in
349 heterocysts relative to vegetative cells. Oscillations are transmitted from the core clock to the
350 *pecBACEF* operon most probably by the master transcription factor RpaA (Arbel-Goren et al.,
351 2021). Here we found that upstream of *pecB* there are two putative RpaA binding sites (p
352 value= 1.5×10^{-5} , Table S1). Since neither the abundance of RpaA nor its transcription decrease as
353 a result of nitrogen deprivation (Camargo et al., 2021; Zhang et al., 2021), lower levels of
354 *pecBACEF* transcription may be effected by a reduction in the levels of the active
355 phosphorylated form (RpaA~P), which may be mediated by SasA and CikA in *Anabaena* as in *S.*
356 *elongatus* (Gutu and O'Shea, 2013). SasA is regulated in *S. elongatus* by the phycobilisome-
357 associated B protein (RpaB), which is involved in the integration of temporal and environmental

358 information and stress (Espinosa et al., 2015). The conservation of the corresponding genes
359 lends support to these notions (Schmelling et al., 2017). Together, these considerations suggest
360 that a link between the circadian clock and the heterocyst differentiation network may be
361 gleaned from the set of genes whose expression is regulated by RpaA~P.

362 Our observation of circadian oscillations in the transcriptional activity of *pecB* in individual
363 heterocysts, together with the inheritance of the phase of oscillation from the primordial
364 vegetative cell lead us to posit that the circadian clock continues to function in the heterocyst,
365 and that rhythmic transcription in the heterocyst is not induced indirectly by time-dependent
366 intercellular signals from clocks in neighboring vegetative cells. While photosystem II (PSII) is
367 altered in heterocysts (Magnuson and Cardona, 2016), PSI continues to function (Magnuson and
368 Cardona, 2016), and the oscillatory behavior of transcriptional activity of *pecB*, even if smaller,
369 suggests that the circadian clock may modulate photosynthetic activity.

370 The sequential turnoff of gene expression according to position along a vegetative cell
371 interval is characterized by timescales that are considerably longer than those typical of
372 intercellular transport of metabolites (Nürnberg et al., 2015), which help maintain filaments in
373 homeostasis. The sequential turnoff here observed is reminiscent of the waves of gene
374 expression measured across different parts of *Arabidopsis thaliana* plants (Endo, 2016; Gould et
375 al., 2018). Nonetheless, the signals coupling clocks are unknown as they are in higher plants
376 (Greenwood and Locke, 2020), and remain to be elucidated.

377 The gating of differentiation by the circadian clock and failure of diazotrophy of $\Delta kaiABC$
378 strains led us to investigate the relationship between these two processes using bioinformatics
379 methodologies. The high conservation of circadian clock components among cyanobacteria
380 (Schmelling et al., 2017), and in particular the high similarity between the protein sequences of
381 RpaA in *Anabaena* and in *S. elongatus*, suggested that RpaA function is conserved as a master
382 clock output regulator. Therefore, we looked for the presence of RpaA putative binding sites
383 upstream of *Anabaena* genes, with low FIMO q-values (i.e., high significance). We found that
384 some of the ChIP-validated genes in *S. elongatus* (Markson et al., 2013), have orthologs in
385 *Anabaena* and have putative binding sites of RpaA. Together, these findings support the notion
386 that RpaA may play a functional role as master regulator of clock outputs in *Anabaena* as in *S.*
387 *elongatus*. However, we have also identified in *Anabaena* putative RpaA controlled genes with
388 specific roles in heterocyst function, which would explain the lack of heterocyst activity in

389 $\Delta kaiABC$ strains. In summary, our work revealed that in *Anabaena* the circadian clock is further
390 necessary to confront nitrogen stress.

391

392 **Materials and Methods**

393 **Strains.** Strains bearing a chromosomally encoded P_{pecB} -*gfp* were obtained by
394 conjugation with the *Anabaena* sp. (also known as *Nostoc* sp.) PCC 7120 wild-type
395 background and with a $\Delta kaiABC$ background, in which the *kaiABC* genes were deleted
396 (Arbel-Goren et al., 2021), as recipients.

397 **Culture conditions.** Strains and derived strains were grown photoautotrophically in
398 BG11 medium containing NaNO_3 , supplemented with 20 mM HEPES (pH 7.5) with
399 shaking at 180 rpm, at 30 °C, as described previously (Corrales-Guerrero et al., 2014,
400 2013). Growth took place under constant illumination ($10 \mu\text{mol m}^{-2}\text{s}^{-1}$) of photons
401 (spectrum centered at 450 nm) from a cool-white LED array. When required,
402 streptomycin sulfate (Sm), and spectinomycin dihydrochloride pentahydrate (Sp) were
403 added to the media at final concentrations of 2 $\mu\text{g}/\text{mL}$ for liquid and 5 $\mu\text{g}/\text{mL}$ for solid
404 media (1% Difco agar); neomycin sulfate (Nm) was added at 10 and 25 $\mu\text{g}/\text{mL}$,
405 respectively. The densities of the cultures were adjusted so as to have a chlorophyll *a*
406 content of 2-4 $\mu\text{g}/\text{mL}$ 24 h prior to the experiment, following published procedures (Di
407 Patti et al., 2018). For time lapse measurements, filaments in cultures were harvested
408 and concentrated 50 fold.

409 **Samples for time-lapse microscopy.** Strains were grown as described previously (Di
410 Patti et al., 2018). When required, antibiotics, streptomycin sulfate (Sm) and
411 spectinomycin dihydrochloride pentahydrate (Sp), were added to the media, at final
412 concentrations of 2 $\mu\text{g}/\text{mL}$ for liquid and 5 $\mu\text{g}/\text{mL}$ for solid media. The densities of the
413 cultures, grown under an external LED array ($15 \mu\text{mol m}^{-2}\text{s}^{-1}$) for about five days, were
414 adjusted so as to have a chlorophyll *a* content of 2-4 $\mu\text{g}/\text{mL}$, 24 h prior to the
415 experiment following published procedures (Di Patti et al., 2018). For time-lapse, single-
416 cell measurements of *Anabaena*, 5 μL of culture concentrated 100-fold were pipetted
417 onto an agarose low-melting gel pad (1.5%) in BG11 medium containing NaNO_3 and 10

418 mM NaHCO₃, which was placed on a microscope slide. The pad with the cells was then
419 covered with a #0 mm coverslip and then placed on the microscope at 30 °C. The cells
420 grew under light from both an external LED array (15 μmol m⁻²s⁻¹) and tungsten halogen
421 light (10 μmol m⁻²s⁻¹), 3000K colour). Under these illumination conditions, the doubling
422 time of cells is similar to that in bulk cultures (Di Patti et al., 2018). The change in
423 illumination conditions when transferring cells from bulk cultures to the microscope
424 results in high synchronization within filaments. Images of about ten different fields of
425 view were taken every 30 min on a Nikon Eclipse Ti-E microscope controlled by the NIS-
426 Elements software using a 60 N.A 1.40 oil immersion phase contrast objective lens
427 (Nikon plan-apochromat 60 1.40) and an Andor iXon X3 EMCCD camera. Focus was
428 maintained throughout the experiment using a Perfect Focus System (Nikon). All the
429 filters used are from Chroma. The filters used were ET480/40X for excitation, T510 as
430 dichroic mirror, ET535/50M for emission (GFP set), ET500/20x for excitation, T515lp as
431 dichroic mirror, and ET535/30m for emission (EYFP set), and ET430/24x for excitation,
432 505dcxt as dichroic mirror, and HQ600lp for emission (chlorophyll set). Samples were
433 excited with a pE- 2 fluorescence LED illumination system (CoolLED).

434 **Image segmentation.** All image processing and data analysis was carried out using
435 Matlab (MathWorks). Filament and individual cell recognition was performed on phase
436 contrast images using an algorithm developed in our laboratory. The program's
437 segmentation was checked in all experiments and corrected manually for errors in
438 recognition. The total fluorescence from GFP and chlorophyll a (autofluorescence)
439 channels of each cell, as well as the cell area, were obtained as output for further
440 statistical analysis.

441 **Analysis of synchronization along filaments.** Synchronization was measured by the
442 order parameter (Garcia-Ojalvo et al., 2004):

$$443 \quad R = \frac{\langle \mu^2 \rangle - \mu^2}{\langle f_i^2 \rangle - \langle f_i \rangle^2} \quad (1)$$

444 where $\langle \cdot \rangle$ denotes a time average, $\bar{\cdot}$ indicates an average over all cells, and μ denotes the
445 average of the fluorescence intensity of each cell f_i . Hence R is defined as the ratio of
446 the standard deviation of $\mu(t)$ to the standard deviation of f_i , averaged over all cells.

447 For measurement of synchronization within the same filament, groups of 8-11 cells
448 were chosen, whether separated or contiguous (sharing a common ancestor as
449 determined from a lineage analysis). For evaluation of inter-filament synchronization,
450 one cell per filament was chosen randomly in different fields of view. R was then
451 calculated and this procedure was repeated for different choices of cells, at least three
452 times for each experiment. All the evaluations of R were carried out over a full period of
453 oscillation, in either one of the first two oscillations, except for the $\Delta kaiABC$ background,
454 for which R was calculated for an interval of 24 hours, during which other strains display
455 the first full oscillation. The final result comprises the mean of at least three
456 independent repeats, in at least two independent experiments. Errors in the quoted
457 values of R therefore represent standard errors (SEM). Statistical analyses were
458 performed in Matlab using Mann-Whitney's U-test.

459 **Identification of RpaA binding motifs in the *Anabaena* genome.** Motif scanning was
460 done using FIMO tool from the MEME Suite (v5.4.1) (Grant et al., 2011), using a
461 previously reported DNA Position-specific probability matrix of the RpaA binding motif
462 in *S. elongatus* (Markson et al., 2013), scanning both strands and reporting a minimal
463 match p-value of 10^{-4} . The results were restricted to sequences within a window of -
464 500bp to +50bp relative to the TSS, based on previously reported *Anabaena* TSS
465 annotations (Mitschke et al., 2011). Assignment of resulting motifs to genes was based
466 on annotations of valid gene names (Mitschke et al., 2011), as well as reported
467 annotations of early and late differentiation genes (cluster #6 and Cluster #4 genes
468 (Brenes-Álvarez et al., 2019)) and (Kushige et al., 2013). Protein sequences coded by
469 *Anabaena* genes, which harbor a putative RpaA motif, were compared with genes
470 reported to bind RpaA in a ChIP experiment in *S. elongatus* (Markson et al., 2013). Thus,
471 protein sequences of 89 reported PCC 7942 genes were compared using BLASTP to
472 *Anabaena* proteins, reporting hits with E-value ≤ 0.005 and $>36\%$ sequence similarity
473 (Table S2).

474

475 **Acknowledgements**

476 Work in Rehovot was supported by the Minerva Stiftung <http://www.minerva.mpg.de/> to JS. JS
477 is the incumbent of a Siegfried and Irma Ullman Professorial Chair. Work in Seville was supported
478 by grant no. PID2020-118595GB-100 from Agencia Estatal de Investigación, Spain, and the
479 European Regional Development Fund to AH and EF.

480

481 **Data availability**

482 Source data files and Matlab code have been deposited in Dryad (DOI
483 https://datadryad.org/stash/share/HOU6G8tz9ugDga2XO_GmaPfNTgfCAYMu8DbI2jFqxUQ).

484

485

486 References

- 487 Arbel-Goren R, Buonfiglio V, Di Patti F, Camargo S, Zhitnitsky A, Valladares A, Flores E, Herrero A,
488 Fanelli D, Stavans J. 2021. Robust, coherent and synchronized circadian clock-controlled
489 oscillations along Anabaena filaments. *Elife* **10**:e64348.
- 490 Arévalo S, Nenninger A, Nieves-Mori6n M, Herrero A, Mullineaux CW, Flores E. 2021.
491 Coexistence of Communicating and Noncommunicating Cells in the Filamentous
492 Cyanobacterium Anabaena. *mSphere* **6**:e01091-20. doi:10.1128/msphere.01091-20
- 493 Asai H, Iwamori S, Kawai K, Ehira S, Ishihara J, Aihara K, Shoji S, Iwasaki H. 2009. Cyanobacterial
494 cell lineage analysis of the spatiotemporal hetR expression profile during heterocyst
495 pattern formation in Anabaena sp. PCC 7120. *PLoS One* **4**:e7371.
- 496 Brenes-Álvarez M, Mitschke J, Olmedo-Verd E, Georg J, Hess WR, Vioque A, Muro-Pastor AM.
497 2019. Elements of the heterocyst-specific transcriptome unravelled by co-expression
498 analysis in *Nostoc* sp. PCC 7120. *Environ Microbiol* **21**:2544–2558. doi:10.1111/1462-
499 2920.14647
- 500 Camargo S, Leshkowitz D, Dassa B, Mariscal V, Flores E, Stavans J, Arbel-Goren R. 2021. Impaired
501 cell-cell communication in the multicellular cyanobacterium Anabaena affects carbon
502 uptake, photosynthesis, and the cell wall. *iScience* **24**:101977.
503 doi:10.1016/j.isci.2020.101977
- 504 Cohen SE. 2020. Circadian Clocks in Cyanobacteria. *Microb Photosynth* 169–180.
505 doi:10.1007/978-981-15-3110-1_9
- 506 Corrales-Guerrero L, Flores E, Herrero A. 2014. Relationships between the ABC-exporter HetC
507 and peptides that regulate the spatiotemporal pattern of heterocyst distribution in
508 Anabaena. *PLoS One* **9**:e104571. doi:10.1371/journal.pone.0104571
- 509 Corrales-Guerrero L, Mariscal V, Flores E, Herrero A. 2013. Functional dissection and evidence
510 for intercellular transfer of the heterocyst-differentiation PatS morphogen. *Mol Microbiol*
511 **88**:1093–1105. doi:10.1111/mmi.12244
- 512 Corrales-Guerrero L, Tal A, Arbel-Goren R, Mariscal V, Flores E, Herrero A, Stavans J. 2015.
513 Spatial Fluctuations in Expression of the Heterocyst Differentiation Regulatory Gene hetR
514 in Anabaena Filaments. *PLoS Genet* **11**:e1005031. doi:10.1371/journal.pgen.1005031
- 515 Di Patti F, Lavacchi L, Arbel-Goren R, Schein-Lubomirsky, L. Fanelli D, Stavans J. 2018. Robust
516 stochastic Turing patterns in the development of a one-dimensional cyanobacterial
517 organism. *PLoS Biol* **16(5)**:e2004877. doi:10.1371/journal.pbio.2004877

- 518 Dong G, Yang Q, Wang Q, Kim Y-I, Wood TL, Osteryoung KW, van Oudenaarden A, Golden SS.
519 2010. Elevated ATPase activity of KaiC applies a circadian checkpoint on cell division in
520 *Synechococcus elongatus*. *Cell* **140**:529–39. doi:10.1016/j.cell.2009.12.042
- 521 Endo M. 2016. Tissue-specific circadian clocks in plants. *Curr Opin Plant Biol*.
522 doi:10.1016/j.pbi.2015.11.003
- 523 Espinosa J, Boyd JS, Cantos R, Salinas P, Golden SS, Contreras A. 2015. Cross-talk and regulatory
524 interactions between the essential response regulator RpaB and cyanobacterial circadian
525 clock output. *Proc Natl Acad Sci U S A* **112**:2198–2203.
526 doi:10.1073/PNAS.1424632112/SUPPL_FILE/PNAS.201424632SI.PDF
- 527 Flores E, Herrero A. 2010. Compartmentalized function through cell differentiation in
528 filamentous cyanobacteria. *Nat Rev Microbiol* **8**:39–50.
- 529 Flores E, Picossi S, Valladares A, Herrero A. 2019. Transcriptional regulation of development in
530 heterocyst-forming cyanobacteria. *Biochim Biophys Acta (BBA)-Gene Regul Mech*
531 **1862**:673–684. doi:10.1016/j.bbagr.2018.04.006
- 532 Foulds IJ, Carr NG. 1977. A proteolytic enzyme degrading phycocyanin in the cyanobacterium
533 *Anabaena cylindrica*. *FEMS Microbiol Lett* **2**:117–119. doi:10.1111/j.1574-
534 6968.1977.tb00921.x
- 535 Garces RG, Wu N, Gillon W, Pai EF. 2004. Anabaena circadian clock proteins KaiA and KaiB reveal
536 a potential common binding site to their partner KaiC. *EMBO J* **23**:1688–1698.
537 doi:10.1038/sj.emboj.7600190
- 538 Garcia-Ojalvo J, Elowitz MB, Strogatz SH. 2004. Modeling a synthetic multicellular clock:
539 repressilators coupled by quorum sensing. *Proc Natl Acad Sci U S A* **101**:10955–60.
540 doi:10.1073/pnas.0307095101
- 541 Gould PD, Domijan M, Greenwood M, Tokuda IT, Rees H, Kozma-Bognar L, Hall AJ, Locke JC.
542 2018. Coordination of robust single cell rhythms in the Arabidopsis circadian clock via
543 spatial waves of gene expression. *Elife* **7**. doi:10.7554/eLife.31700
- 544 Grant C, Bailey T, Noble W. 2011. FIMO: scanning for occurrences of a given motif.
545 *Bioinformatics* **27**:1017–1018.
- 546 Greenwood M, Locke JC. 2020. The circadian clock coordinates plant development through
547 specificity at the tissue and cellular level. *Curr Opin Plant Biol*.
548 doi:10.1016/j.pbi.2019.09.004
- 549 Gutu A, O’Shea EK. 2013. Two Antagonistic Clock-Regulated Histidine Kinases Time the

- 550 Activation of Circadian Gene Expression. *Mol Cell* **50**:288–294.
551 doi:10.1016/J.MOLCEL.2013.02.022
- 552 Herrero A, Stavans J, Flores E. 2016. The multicellular nature of filamentous heterocyst-forming
553 cyanobacteria. *FEMS Microbiol Rev* **40**:831–854. doi:10.1093/femsre/fuw029
- 554 Johnson C, Rust M, editors. 2021. Circadian Rhythms in Bacteria and Microbiomes. Springer.
- 555 Kushige H, Kugenuma H, Matsuoka M, Ehira S, Ohmori M, Iwasaki H. 2013. Genome-wide and
556 heterocyst-specific circadian gene expression in the filamentous Cyanobacterium
557 *Anabaena* sp. strain PCC 7120. *J Bacteriol* **195**:1276–84. doi:10.1128/JB.02067-12
- 558 Magnuson A, Cardona T. 2016. Thylakoid membrane function in heterocysts. *Biochim Biophys*
559 *Acta - Bioenerg* **1857**:309–319. doi:10.1016/J.BBABIO.2015.10.016
- 560 Maldener I, Lockau W, Cai Y, Wolk CP. 1991. Calcium-dependent protease of the
561 cyanobacterium *Anabaena*: molecular cloning and expression of the gene in *Escherichia*
562 *coli*, sequencing and site-directed mutagenesis. *Mol Gen Genet MGG* **225**:113–120.
563 doi:10.1007/BF00282649
- 564 Markson J, Piechura J, Puszynska A, O’Shea E. 2013. Circadian Control of Global Gene Expression
565 by the Cyanobacterial Master Regulator RpaA. *Cell* **155**:1396–1408.
- 566 Mella-Herrera RA, Neunuebel MR, Kumar K, Saha SK, Golden JW. 2011. The sigE gene is required
567 for normal expression of heterocyst-specific genes in *Anabaena* sp. strain PCC 7120. *J*
568 *Bacteriol* **193**:1823–1832. doi:10.1128/JB.01472-10/SUPPL_FILE/MOVIE_LEGENDS.DOC
- 569 Mitschke J, Vioque A, Haas F, Hess WR, Muro-Pastor AM. 2011. Dynamics of transcriptional start
570 site selection during nitrogen stress-induced cell differentiation in *Anabaena* sp. PCC7120.
571 *Proc Natl Acad Sci USA* **108**:20130–20135.
572 doi:10.1073/PNAS.1112724108/SUPPL_FILE/SD01.XLSX
- 573 Nieves-Mori3n M, Flores E, Whitehouse MJ, Thomen A, Foster RA. 2021. Single-cell
574 measurements of fixation and intercellular exchange of c and n in the filaments of the
575 heterocyst-forming cyanobacterium *Anabaena* sp. Strain pcc 7120. *MBio* **12**:e01314-21.
576 doi:10.1128/MBIO.01314-21/ASSET/1B820C73-04BD-4CFF-9126-
577 21A78BD2AF25/ASSETS/IMAGES/MEDIUM/MBIO.01314-21-F011.GIF
- 578 N3rnberg DJ, Mariscal V, Bornikoel J, Nieves-Mori3n M, Krauß N, Herrero A, Maldener I, Flores E,
579 Mullineaux CW. 2015. Intercellular diffusion of a fluorescent sucrose analog via the septal
580 junctions in a filamentous cyanobacterium. *mBio* **6**:e02109. doi:10.1128/mBio.02109-14
- 581 Sarasa-Buisan C, Guio J, Broset E, Peleato ML, Fillat MF, Sevilla E. 2022. FurC (PerR) from

- 582 Anabaena sp. PCC7120: a versatile transcriptional regulator engaged in the regulatory
583 network of heterocyst development and nitrogen fixation. *Environ Microbiol* **24**:566–582.
584 doi:10.1111/1462-2920.15552
- 585 Schmelling NM, Lehmann R, Chaudhury P, Beck C, Albers S-V, Axmann IM, Wiegard A. 2017.
586 Minimal tool set for a prokaryotic circadian clock. *BMC Evol Biol* **17**:169.
587 doi:10.1186/s12862-017-0999-7
- 588 Shultzaberger RK, Boyd JS, Diamond S, Greenspan RJ, Golden SS. 2015. Giving Time Purpose: The
589 *Synechococcus elongatus* Clock in a Broader Network Context. *Annu Rev Genet* **49**:485–
590 505. doi:10.1146/annurev-genet-111212-133227
- 591 Suzuki T, Yoshimura H, Hisabori T, Ohmori M. 2004. Two cAMP receptor proteins with different
592 biochemical properties in the filamentous cyanobacterium *Anabaena* sp. PCC 7120. *FEBS*
593 *Lett* **571**:154–160. doi:10.1016/J.FEBSLET.2004.06.074
- 594 Swanson R, Lorimier R de, Glazer A. 1992. Genes encoding the phycobilisome rod substructure
595 are clustered on the *Anabaena* chromosome: characterization of the phycoerythrocyanin
596 operon. *J Bacteriol* **174**:2640–2647.
- 597 Taniguchi Y, Takai N, Katayama M, Kondo T, Oyama T. 2010. Three major output pathways from
598 the KaiABC-based oscillator cooperate to generate robust circadian kaiBC expression in
599 cyanobacteria. *Proc Natl Acad Sci U S A* **107**:3263–8. doi:10.1073/pnas.0909924107
- 600 Taton A, Erikson C, Yang Y, Rubin B, Rifkin S, Golden J, Golden S. 2020. The circadian clock and
601 darkness control natural competence in cyanobacteria. *Nat Commun* **11**:1688.
- 602 Wood NB, Haselkorn R. 1980. Control of phycobiliprotein proteolysis and heterocyst
603 differentiation in *Anabaena*. *J Bacteriol* **141**:1375–1385.
- 604 Yang Q, Pando BF, Dong G, Golden SS, van Oudenaarden A. 2010. Circadian gating of the cell
605 cycle revealed in single cyanobacterial cells. *Science* **327**:1522–6.
606 doi:10.1126/science.1181759
- 607 Zhang Q, Yu S, Wang Q, Yang M, Ge F. 2021. Quantitative Proteomics Reveals the Protein
608 Regulatory Network of *Anabaena* sp. PCC 7120 under Nitrogen Deficiency. *Cite This J*
609 *Proteome Res* **20**:3963–3976. doi:10.1021/acs.jproteome.1c00302
- 610

611

Supporting files

612

613 **Movie 1.** Circadian oscillations in *Anabaena* filaments under nitrogen-poor conditions as a
614 function of time.

615 **Figure S1.** Genetic structure in the $\Delta kaiABC$ mutants.

616 **Figure S2.** Heterocyst formation in the Δkai mutants of *Anabaena* sp. strain PCC 7210.

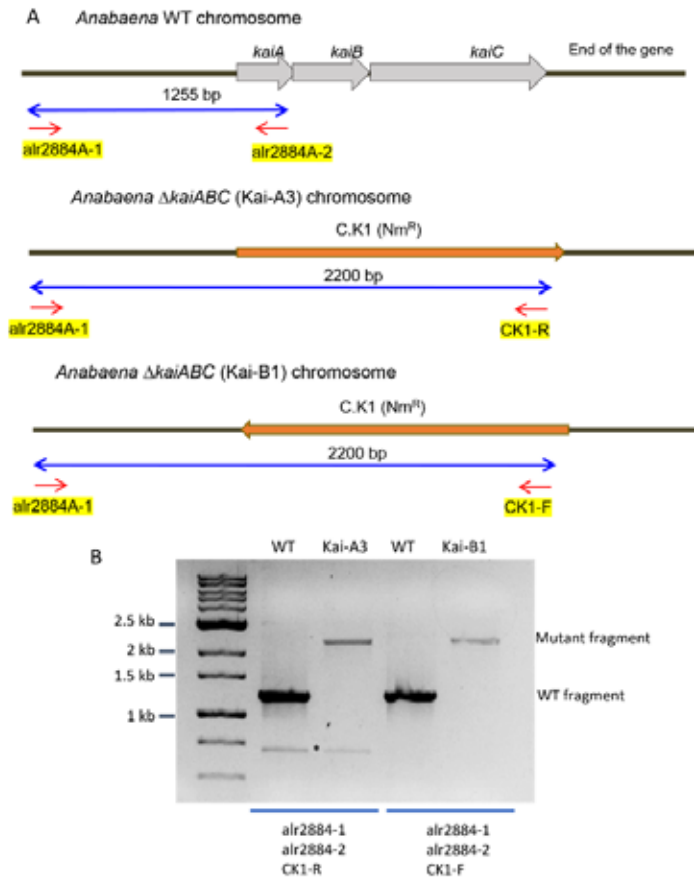
617 **Table S1.** RpaA putative binding motifs identified in *Anabaena* sp. strain PCC 7120 including
618 FIMO statistics and additional annotations.

619 **Table S2.** BLASTP analysis of *S. elongatus* orthologous proteins to *Anabaena* sp. strain PCC 7120.

620

621

622



623

624

Figure S1. Genetic structure in the Δ *kaiABC* mutants. The Δ *kaiABC* mutants were re-isolated following the procedure described in Arbel-Goren *et al.*, 2021, but now the gene-cassette, C.K1, was inserted in both orientations (direct orientation, mutants A; opposite orientation, mutants B). (A) The genetic structure in the *kai* genomic region is shown for the wild type (top scheme), a mutant with the gene cassette in direct orientation (middle) and a mutant with the gene cassette in opposite orientation (bottom). Oligonucleotide primers used in PCR analysis are indicated. (B) PCR analysis with genomic DNA isolated from the wild type or the A3 and B1 *kai* mutants grown in BG11 medium (with neomycin at 20 μ g mL⁻¹ for the mutants) and incubated for 48 h in BG11₀ medium (without neomycin). Three primers were added to each reaction, as indicated, resulting in amplification of only WT DNA fragments in the wild type and only mutant fragments in the mutants, indicating segregation of the mutant chromosomes. *, non-specific amplification product.

625

626

627

628

629

630

631

632

633

634

635

636

637

638

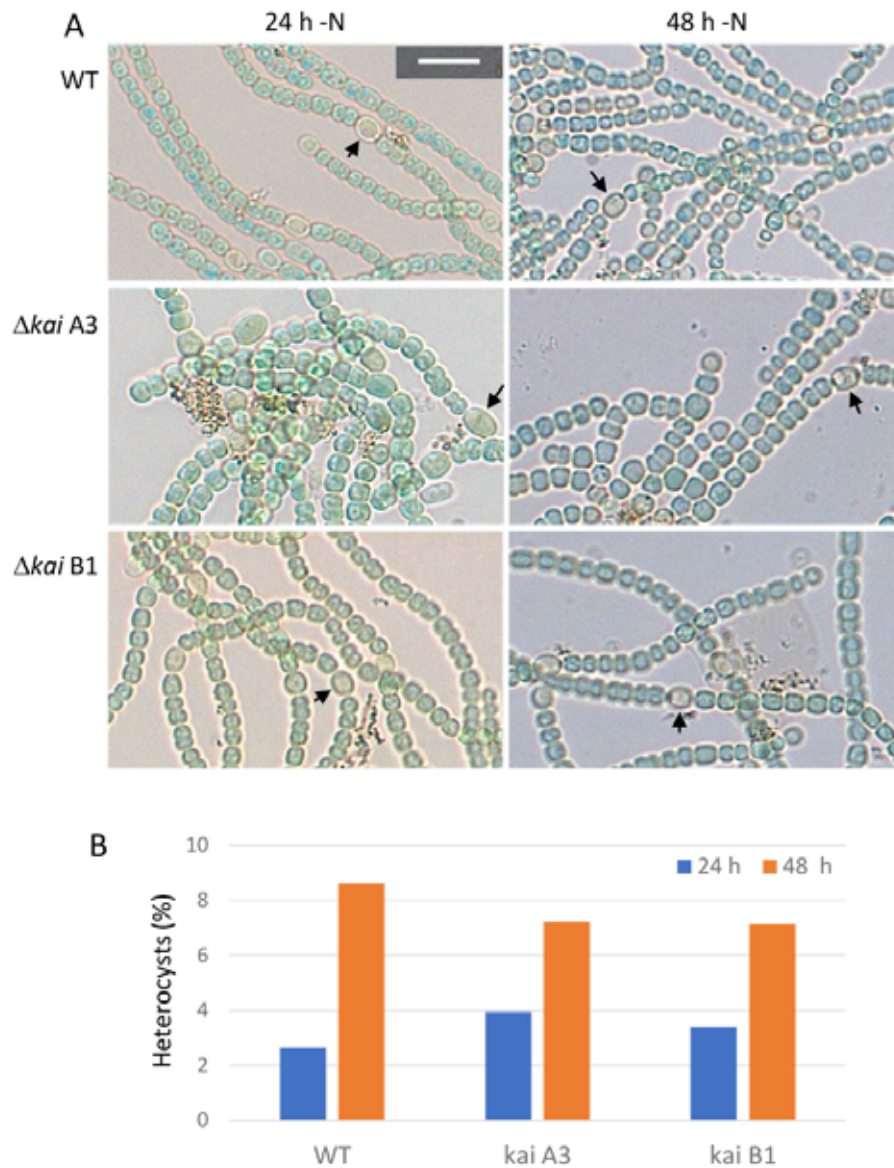
639

640

641

642

643
644



645 **Figure S2. Heterocyst formation in the Δkai mutants of *Anabaena* sp. strain PCC 7210.** The
646 strains were grown in BG11 medium (in the presence of neomycin at $20 \mu\text{g mL}^{-1}$ for the
647 mutants), washed with BG11₀ medium and incubated in liquid BG11₀ medium (without
648 antibiotic) under photoautotrophic culture conditions for 24 and 48 h, respectively. (A)
649 Examples of filaments showing the presence of heterocysts (some indicated by black arrows).
650 Size bar, 10 μm ; same magnification in all the micrographs. (B) Heterocysts as percentage of
651 total number of cells in the three strains after 24 or 48 h of incubation in BG11₀ medium. Total
652 number of cells counted: 1300 to 1500 in the 24-h samples; 1000 to 1100 in the 48-h samples.